論文 / 著書情報
Article / Book Information

論題(和文)	
Title(English)	Seismic response of high-rise building with viscous dampers considering its performance decrement under long-period ground motion
著者(和文)	劉 錫媛, 佐藤 大樹
Authors(English)	Xiyuan Liu, Daiki Sato
出典(和文)	, , , pp. 50-57
Citation(English)	Proceedings of the 6th Joint Workshop on Building / Civil Engineering between Tokyo Tech & Tongji, , , pp. 50-57
発行日 / Pub. date	2019, 5

The 6th Joint Workshop on Building / Civil Engineering between Tokyo Tech & Tongji
May 31 – June 1, 2019, Tongji University, Shanghai, China

SEISMIC RESPONSE OF HIGH-RISE BUILDING WITH VISCOUS DAMPERS CONSIDERING ITS PERFORMANCE DECREMENT UNDER LONG-PERIOD GROUND MOTION

Xiyuan Liu[1], Daiki Sato[2]

1) Graduate student, Department of Architecture and Building Engineering, Tokyo Institute of Technology, Yokohama, Japan
2) Associate professor, Laboratory for Future Interdisciplinary Research of Science and Technology (FIRST), Tokyo Institute of Technology, Yokohama, Japan

Abstract: This paper presents the seismic response of 20-story building with viscous dampers considering the performance decrement under long-period ground motion by using three analysis methods, including story drift angle, absolute acceleration, absorbed energy of individual viscous damper, the absorbed energy of total viscous dampers, the damping energy of structure, and the energy distribution rate of dampers. The three analysis methods, conventional method, simplified method, and detailed method, were also assessed. The simplified method is the most valuable amongst the three methods. Two types of viscous dampers are evaluated by using energy density and decrease rate, medium capacity dampers and large capacity dampers. The performance decrement of large volume dampers are less than medium capacity dampers. In addition, the story drift is the larger, the decrease rate is the smaller.

1. INTRODUCTION

Long-period ground motions due to potential Nankai Trough earthquakes are expected to be generated which will attack the three major metropolitans in Japan, i.e., Tokyo, Osaka, and Nagoya. It is feared that high-rise buildings with long natural periods will be severely affected. The passive control device is effective in mitigating such damage. The viscous damper targeted in this study is a flow resistance type damper which used the flow resistance force of the enclosed fluid. However, while vibration energy is converted into thermal energy, the temperature of the viscous fluid increased and the damper performance decreased. Therefore, a design method for vibration control buildings needs to consider the characteristic decrease of viscous dampers under long-period ground motion.

The design of the structure with viscous dampers is based on the response of time history analysis and energy analysis [Akiyama, 1999]. Kasai et al. [2017] performed long-term sinusoidal wave excitation tests on full-scale viscous dampers. They proposed a performance decrease evaluation method using energy density which is the cumulative absorbed energy divided by the volume of the viscous fluid. Nagayama et al [2017a,b] proposed the simplified response evaluation of vibration control building with viscous damper that considered the performance decrement caused by long-period cyclic loading. Sato et al [2018a] assesses the three analysis method, the conventional methods, simplified method, and detailed method, and researched the decrease rate using the simplified method by SDOF model. The main frame is elastic. The simplified method which is not considering the cyclic decrease rate is the most valuable amongst the three method. Okada, R. and Sato, D. [2018b] examined the validity of the simplified method which considered the plasticity of the structure by MDOF model. The influence of the performance decrement of dampers is smaller than the case the main frame of which is elastic. Okada, R. and Sato, D. [2018c,d] analyzed on the energy of passive structure with dampers, and verified accuracy of energy distribution by MDOF model.

This paper presents the seismic response of 20-story building with viscous dampers considering the performance decrement under long-period ground motion by using 3D model through the response of time history analysis and energy analysis. In section 2, the summary of viscous dampers and the building are presented. The structure is elastic. The effect of bending deformation is not considered. Moreover, the analysis model of viscous dampers considering performance decrement is proposed. In section 3, the input ground motion is presented. In section 4, the three analysis methods, conventional method, simplified method, and detailed method, were assessed by story drift angle and absolute acceleration. In section 5, the decrease rate is analyzed, including energy, the decrease rate of the two types of dampers and the decrease rate in three analysis methods.

2. SUMMARY OF DAMPERS AND BUILDING

2.1 Viscous Dampers

Two types of viscous damper, medium capacity damper and large capacity damper, are distributed in this paper. The velocity index α and the viscous coefficient C_d of the viscous dampers are presented in Table 1[Kasai et al. 2017]. Since the damper and the support member are connected in series (Figure 1), the internal stiffness K_d and support member stiffness K_b are shown by the equivalent stiffness (Table 1) K_b^*[Sato et al. 2018].

Table 1 Parameter of viscous damper

object	α	C_d[kN·(s/mm)$^\alpha$]	K_d[kN/cm]	K_b[kN/cm]	K_b^*[kN/cm]
D2-2F	0.38	98	2663	2525	1296
D3-2F	0.38	196	4858	4842	2425

※D2-2F is Medium capacity, D3-2F is Large capacity.

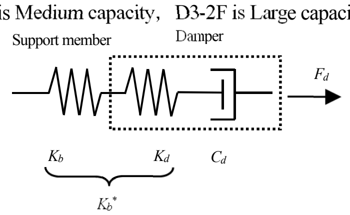

Figure 1 damper and support member

2.2 Analysis Model Considering Performance Decrement of Viscous Damper

The force of the viscous damper in step n $F_d^{(n)}$, is expressed by equation (1):

$$F_d^{(n)} = C_d^{(n)} \cdot \left|\dot{u}_d^{(n)}\right|^{\alpha} \operatorname{sgn}(\dot{u}_d^{(n)}) \tag{1}$$

where $\dot{u}_d^{(n)}$ is the velocity at n step; $C_d^{(n)}$ is the viscous coefficient at n step. $C_d^{(n)}$ considering its repeated effects is calculated by equation (2) [Kasai et al. 2017].The decrease rate $\lambda^{(n)}$ of the viscous coefficient due to the repeated effects is defined by equation (3) [Kasai et al. 2017].

$$C_d^{(n)} = \lambda^{(n)} \cdot C_d^{(0)} \tag{2}$$

$$\lambda^{(n)} = \exp(-a_0 \cdot \Omega^{(n)}) \tag{3}$$

where $C_d^{(0)}$ is the initial value of the viscous coefficient; a_0 is the value depending on the standard of the damper, which can be calculated from a long-term excitation experiment. In this paper a_0=1.695×10^{-6} m^2/kN[Kasai et al. 2017] is used. $\Omega^{(n)}$ is the energy density at n step, which is described by the following equation (4) [Kasai et al. 2017]:

$$\Omega^{(n)} = \frac{w_d^{(n)}}{V_V} \tag{4}$$

where $w_d^{(n)}$ is the cumulative absorbed energy up to the n step of the damper, V_V and is the volume of the viscous fluid. The V_V of medium capacity damper is 0.0083436m^3, and the V_V of large capacity damper is 0.024823712 m^3 [Kasai et al. 2017].

Figure 2 [Nagayama et al. 2017] presents the long-term excitation experiment results and the analytical results. The period of the sinusoidal wave is 4.0s, the amplitude of the sinusoidal wave is 20mm. It can be verified that the analysis model can reproduce the tendency of the performance decrement with each cycle with high accuracy.

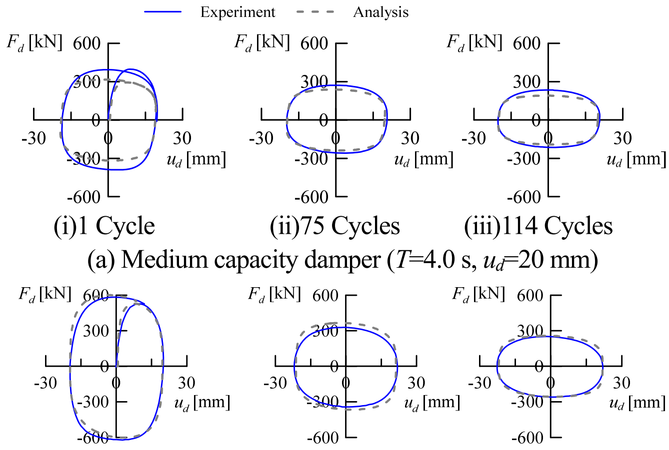

(i)1 Cycle (ii)75 Cycles (iii)114 Cycles

(a) Medium capacity damper (T=4.0 s, u_d=20 mm)

(i)1 Cycle (ii)225 Cycle (iii)449 Cycles

(b) Large capacity damper (T=4.0 s, u_d=20 mm)

Figure 2 Comparison between experiment and analysis result

2.3 Building

The height of the steel building is 81.7m, 20-story [AIJ. 2017]. The height of the first floor is 6.0m, the others are 4.0m. Table 2 presents the column section list. In order to avoid the early yielding of the connection panel, the thickness of parts of the panel is made thicker than the thickness of the column. Table 3 presents the thickness of the panel. The long side direction of the structure is the X direction, and the short side direction is the Y direction. The X direction is considered. Figure 3 presents the plan and elevation of the building. The 1st and 2nd period T_f (X direction) is 2.29s and 0.81s. The structure is elastic.

The Rayleigh damping is selected. The damping ratio for the 1st and 2nd modes are 1.5% and 1.95%. The mass-proportional coefficient a_M and a_K stiffness-proportional coefficient are defined by equation (5) and (6). In this paper, a_M=0.05060, a_K=0.00421.

$$a_M = \frac{2\omega_1\omega_2(h_1\omega_2 - h_2\omega_1)}{(\omega_2^2 - \omega_1^2)} \tag{5}$$

$$a_K = \frac{2(h_2\omega_2 - h_1\omega_1)}{(\omega_2^2 - \omega_1^2)} \tag{6}$$

Table 2 Column list (unit[mm])

Story	C1	C2	C3
17~20	550×550×25	500×500×22	500×500×19
13~16	600×600×28	550×550×25	500×500×19
9~12	650×650×28	600×600×28	550×550×22
6~8	650×650×32	600×600×28	600×600×25
4~5	700×700×32	650×650×28	650×650×28
2~3	750×750×36	700×700×36	700×700×32
1	800×800×36	750×750×36	750×750×32

Table 3 Panel list (unit [mm])

Floor	C1	C2	C3
R~20	28	22	19
19~18	32	25	19
17~15	32	25	22
14~12	32	32	25
11~10	28	28	22
9~7	32	28	25
6~5	32	32	28
4~2	36	36	32

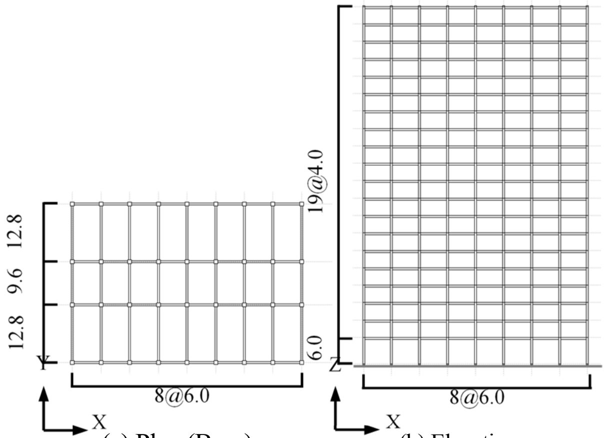

(a) Plan (Base) (b) Elevation

Figure 3 Plan and Elevation (unit[m])

2.4 Distribution of Viscous Dampers

There are 4 types of damper distribution: $_{M}$R100、$_{L}$R100、$_{M}$R150、$_{L}$R150.In addition, the damper of D2-2F (Medium capacity damper) in Table 1 adds the letter "M" to the left, and D3-2F(Large capacity damper) is "L". Under lever 2 seismic ground motion (Art-Hachi), the story drift angle R of the structure with $_{M}$R100、$_{L}$R100 is less than 1/100, and the story drift angle R of the structure with $_{M}$R150、$_{L}$R150 is less than 1/150. Figure 4 presents the viscous coefficient in the height direction. Table 4 presents the number of viscous dampers in each story. Figure 5~ Figure 8 presents the plan and elevation with dampers in the X direction.

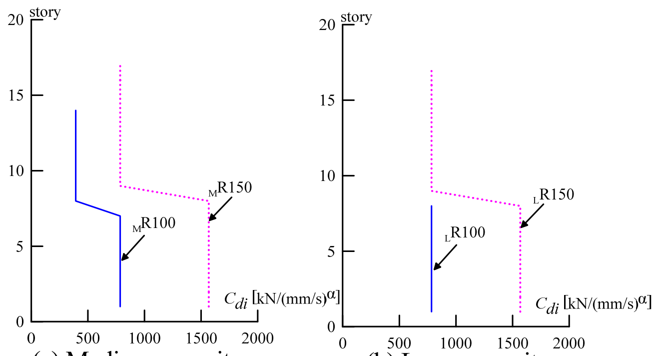

(a) Medium capacity (b) Large capacity

Figure 4 Viscous coefficient

Table 4 Amount of viscous dampers

Story	$_{M}$R100	$_{M}$R150	$_{L}$R100	$_{L}$R150
18~20	0	0	0	0
15~17	0	8	0	4
9~14	4	8	0	4
8	4	16	4	8
1~7	8	16	4	8

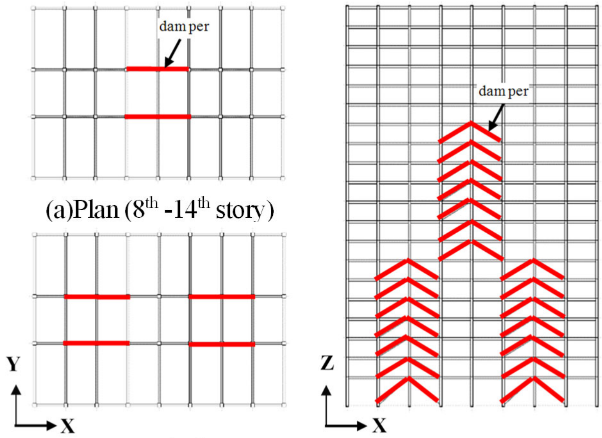

(a)Plan (8th -14th story)

(b)Plan (1st-7th story) (c) Elevation

Figure 5 Plan and elevation with $_{M}$R100

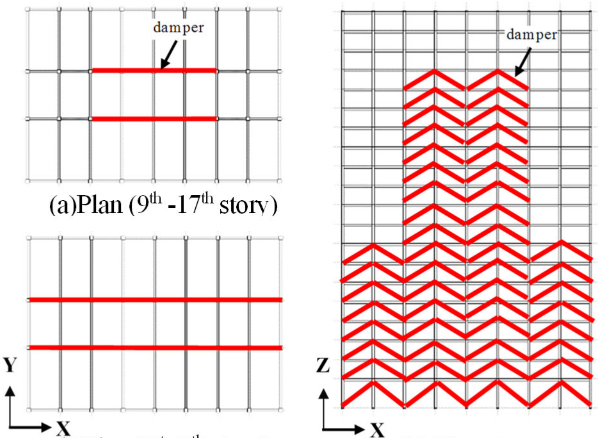

(a)Plan (9th -17th story)

(b)Plan (1st -8th story) (c) Elevation

Figure 6 Plan and elevation with $_{M}$R150

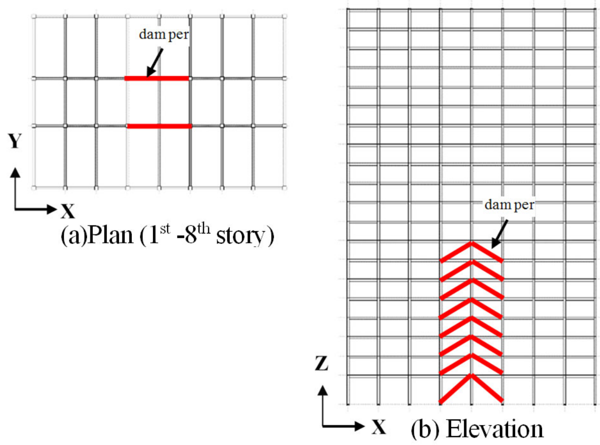

(a)Plan (1st -8th story)

(b) Elevation

Figure 7 Plan and elevation with $_{L}$R100

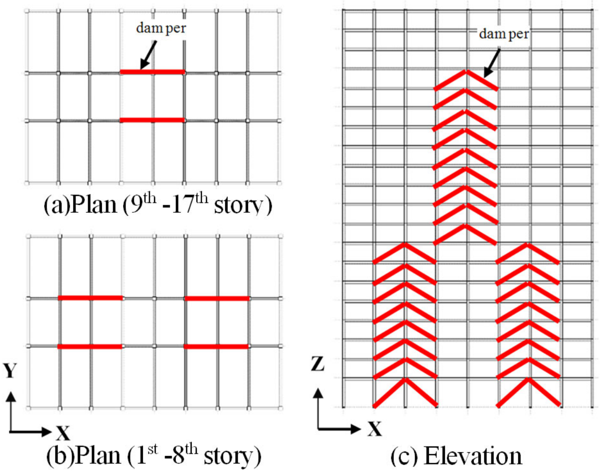

Figure 8 Plan and elevation with $_L$R150

3. INPUT GROUND MOTION

Two earthquakes were adopted in this paper: Art-Hachi (phase value: HACHINOHE 1968 EW), which is equivalent to the design earthquake of level 2, and the long-period ground motion CH1 [BRI 2017]. The S_v (h = 5 %) of level 2 is 100cm/s after the corner period T_c=0.64s. Figure 9 presents the acceleration of earthquakes. Figure 10 presents the pseudo-velocity response spectrum $_pS_v$ (h = 5 %) and energy spectrum V_E (h = 10 %). From Figure 10, it can be seen that the $_pS_v$ of CH1 is about 1.5 times larger than Art-Hachi, V_E of CH1 is about 2.1times larger than Art-Hachi.

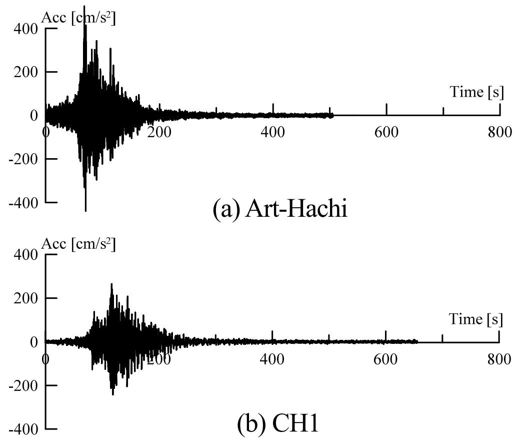

Figure 9 Acceleration of earthquake

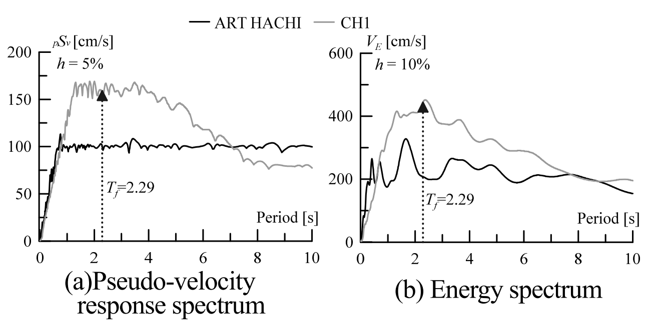

Figure 10 Response spectrum

4. TIME HISTORY RESPONSE ANALYSIS

Three types of analysis methods are used in the time history response analysis: conventional method, simplified method, and detailed method. The conventional method is to use the initial value of the viscous coefficient $C_d^{(0)}$ for analysis. The simplified method is based on the energy density Ω (equation 4) of the conventional method at the end of the earthquake, and the decrease rate λ can be calculated from energy density Ω (equation 3). After that, the initial value of the viscous coefficient $C_d^{(0)}$ is multiplied by a decrease rate λ (equation 2), then do the analysis again by using viscous coefficient C_d. Figure 11 presents the flowchart for the simplified method. The detailed method is to calculate the decrease rate λ (equation 2) of each step, and then the analysis is carried out.

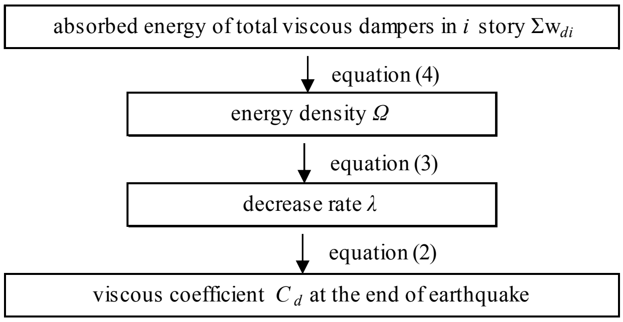

Figure 11 Flowchart for simplified method

4.1 Analysis of Art-Hachi

The story drift angle R under Art-Hachi is presented is Figure 12. From figure 12, it can be seen that $_M$R100、$_L$R100 schemes achieve story drift angle R less than 1/100, and $_M$R150、$_L$R150 schemes achieve story drift angle R less than 1/150.

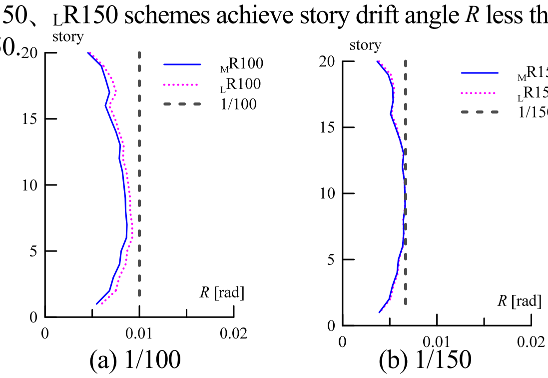

Figure12 Story drift angle (Art-Hachi)

4.2 Analysis of Medium Capacity Damper

Figure 13 presents the maximum story drift angle R, and the maximum absolute acceleration Acc. at the end of the earthquake. From figure 13, it can be seen that the conventional method< detailed method < simplified method. Since the response of the simplified method is larger than the detailed method without cycling each step, the simplified method is the most valuable amongst the three methods. It can be seen the same tendency in absolute acceleration Acc.

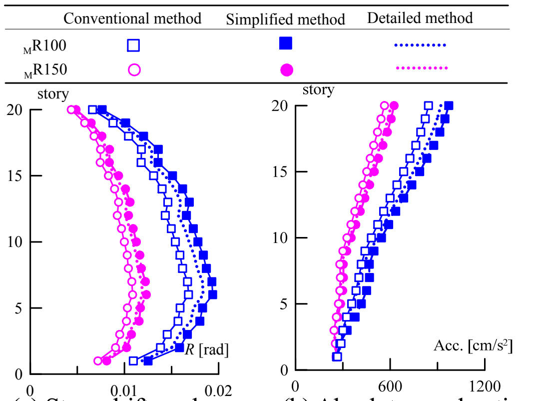

(a) Story drift angle (b) Absolute acceleration

Figure 13 Medium capacity dampers (CH1)

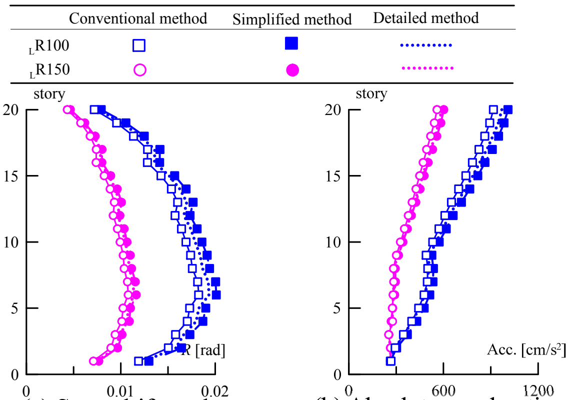

(a) Story drift angle (b) Absolute acceleration

Figure 14 Large volume dampers (CH1)

4.3 Analysis of Large Capacity Damper

Figure 14 presents the maximum story drift angle R, and absolute acceleration Acc. at the end of the earthquake. From figure 14, it can be seen that the same tendency as section 4.2.

5. DECREASE RATE

5.1 Analysis of Energy

Figure 15 presents the absorbed energy of individual viscous damper w_d in i story at the end of earthquake. From figure 15, for $_{\mathrm{M}}$R100 it is shown that simplified method < detailed method <conventional method. For $_{\mathrm{M}}$R150, because the performance decrement is small, w_d is almost the same in each method. Moreover, the absorbed energy w_d of $_{\mathrm{M}}$R100 is about 2.0～2.3 times greater than $_{\mathrm{M}}$R150, since the volume of the viscous fluid V_V is the same, the decrease rate λ of $_{\mathrm{M}}$R100 is about 0.79 times less than $_{\mathrm{M}}$R150. In addition, it can be seen that w_d of $_{\mathrm{L}}$R150 is about 2.0 times greater than $_{\mathrm{M}}$R150.

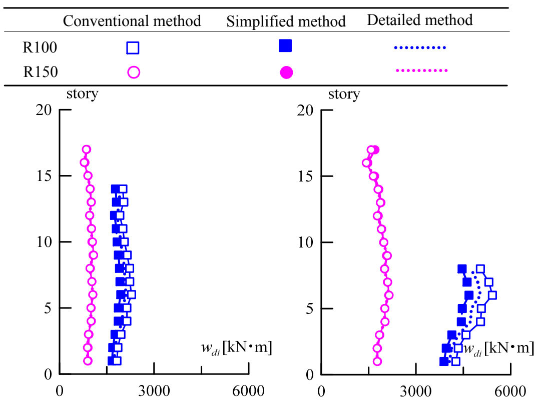

(a) Medium capacity (b) Large capacity

Figure 15 Absorbed energy of individual viscous damper (CH1)

Figure 16 presents the damping energy of structure W_{fh} and the absorbed energy of total viscous dampers W_d at the end of the earthquake. From figure 16(a), because of the performance decrement, for W_d it is shown that the simplified method < detailed method < conventional method. W_d in the detailed method is 0.94 times less than the conventional method, and 1.06 times greater than the simplified method. From figure 16(b), because the performance decrement is small, W_d is almost the same in each method for $_{\mathrm{M}}$R150. From figure 16 and figure 15(a), it is shown that W_d of $_{\mathrm{M}}$R150 is greater than $_{\mathrm{M}}$R100, however, the amount of $_{\mathrm{M}}$R150 is more, so the absorbed energy of individual viscous damper w_d is less than $_{\mathrm{M}}$R100.

Table 5 presents the energy distribution rate of dampers W_d/E. E is the input energy of the earthquake. From table 5, it can be seen that the W_d/E of $_{\mathrm{M}}$R100 is about 40%, $_{\mathrm{M}}$R150 is about 70%. The W_d/E of $_{\mathrm{M}}$R150 is less than $_{\mathrm{M}}$R100.

Figure 17 presents the damping energy of structure W_{fh} and the absorbed energy of total viscous dampers W_d at the end of the earthquake. Table 6 presents the energy distribution rate W_d/E. From figures and table 6, it can be seen the same tendency as medium capacity dampers.

5.2 Decrease Rate about Two Types of Dampers

Figure 18 presents the absorbed energy Σw_{di} of dampers in i story. Figure 19 presents the energy density Ω defined by equation (4) in the height direction, and figure 20 presents the decrease rate λ defined by equation (3) in the height direction at the end of the earthquake. From figure 18, it is shown that the absorbed energy Σw_{di} of $_{\mathrm{L}}$R100 is the largest. From figure 19 and figure 20, it is shown that the energy density Ω of $_{\mathrm{M}}$R100 is the largest, about 1.5 times larger than $_{\mathrm{L}}$R150. However, the volume of viscous fluid V_V in large capacity is about 3.0 times larger than the medium capacity damper, so the decrease rate λ of $_{\mathrm{L}}$R150 is the largest. The performance decrement of $_{\mathrm{L}}$R150 is the least. Moreover, from figure 20, it is shown that the decrease rate of $_{\mathrm{M}}$R100 is about 0.65, $_{\mathrm{L}}$R100 is about 0.72, $_{\mathrm{M}}$R150 is about 0.81, $_{\mathrm{L}}$R150 is about 0.89. Compared the decrease rate λ of $_{\mathrm{M}}$R100 with $_{\mathrm{L}}$R100 , and the decrease rate λ of $_{\mathrm{M}}$R150 with $_{\mathrm{L}}$R150 , it is shown that the decrease rate λ of $_{\mathrm{L}}$R100 is larger than $_{\mathrm{M}}$R100 ,and $_{\mathrm{L}}$R150 is the larger than $_{\mathrm{M}}$R150 , so with the uniform story drift angle constraints, the decrease rate λ of the large capacity damper is larger than medium capacity damper. In addition, compared the decrease rate λ of $_{M}$R100 with $_{M}$R150, and the λ of $_{L}$R100 with $_{L}$R150, it is shown that the λ of $_{M}$R150 is the larger than $_{M}$R100,and the λ $_{L}$R150 is the larger than $_{L}$R100, with the uniform volume constraints, so story drift angle 1/150 is more valuable than 1/100. Since the height of the two story is the same, the story drift is the larger, the decrease rate is the smaller.

Figure 21～22 presents the hysteresis loop of individual damper of $_{M}$R100 and $_{L}$R150 in 6th story under CH1. From figure 21 and figure 22, it is can be seen that the performance decrement of $_{M}$R100 is large, the performance decrement of $_{L}$R150 is small.

5.3 Decrease Rate about Three Analysis Methods

Figure 23～24 presents the time history of the decrease rate λ of $_{M}$R100 and $_{L}$R150. From figure 23, it can be seen that λ of the 6th story is lower than 2nd story, since the story drift of the 6th story is larger than 2nd story, the decrease rate λ is smaller. From figure 23 and figure 24, it can be seen that the decrease rate λ of $_{L}$R150 is larger than $_{M}$R100, which is the same with figure 20.

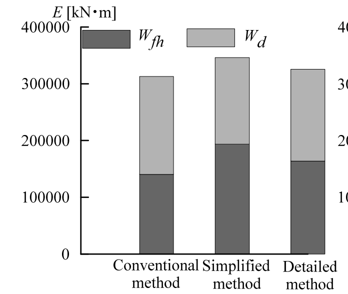

(a) $_{M}$R100

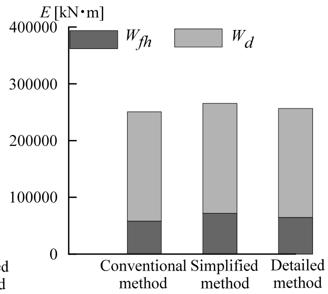

(b) $_{M}$R150

Figure 16 Absorbed energy of total viscous dampers and damping energy of structure (CH1)

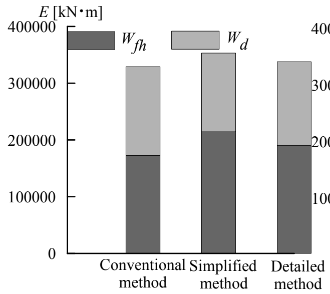

(a) $_{L}$R100

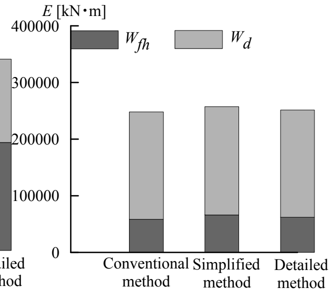

(b) $_{L}$R150

Figure 17 Absorbed energy of total viscous dampers and damping energy of structure (CH1)

Table 5 Energy proportion of W_d/E (CH1) (Medium capacity damper)

	$_{M}$R100	$_{M}$R150
Conventional method	0.55	0.77
Simplified method	0.44	0.73
Detailed method	0.50	0.75

Table 6 Energy proportion of W_d/E (CH1) (Large capacity damper)

	$_{L}$R100	$_{L}$R150
Conventional method	0.47	0.76
Simplified method	0.39	0.74
Detailed method	0.44	0.75

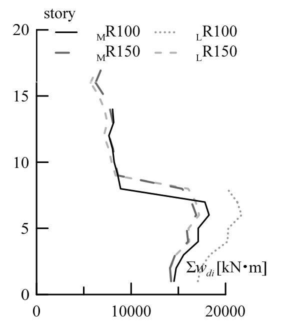

Figure.18 Absorbed energy of viscous damper(CH1)

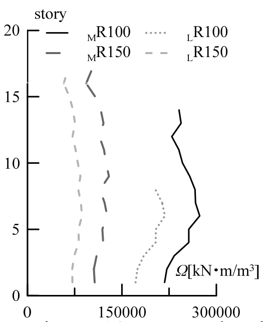

Figure.19 Energy density (CH1)

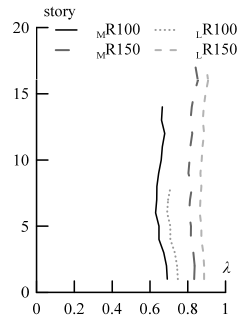

Figure.20 Decrease rate (CH1)

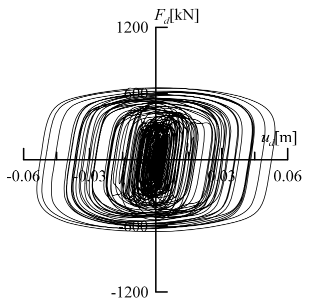

(a) Conventional method

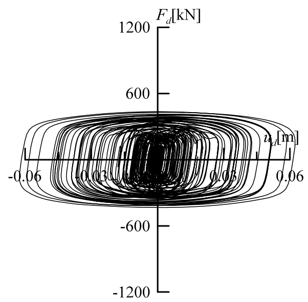

(b) Simplified method

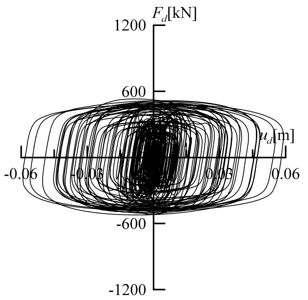

(c) Detailed method

Figure 21 Hysteresis loop of $_{M}$R100 under CH1 (6th story)

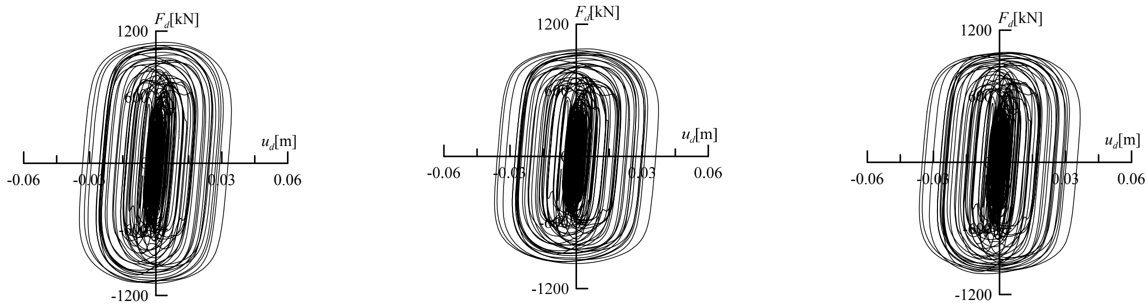

(a) Conventional method (b) Simplified method (c) Detailed method

Figure 22 Hysteresis loop of $_{\mathrm{L}}$R150 under CH1 (6th story)

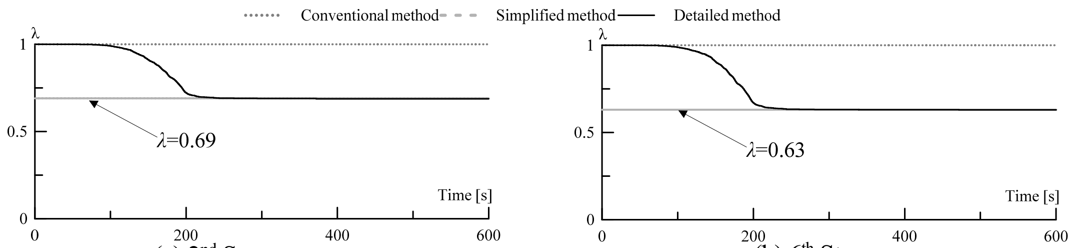

(a) 2nd Story (b) 6th Story

Figure 23 Time history of decrease rate of $_{\mathrm{M}}$R100 (CH1)

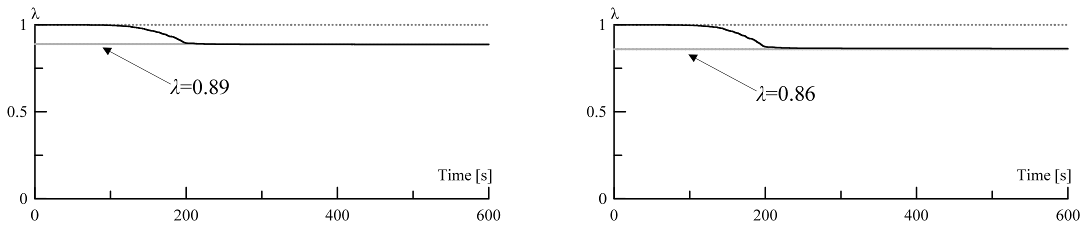

(a) 2nd Story (b) 6th Story

Figure 24 Time history of decrease rate of $_{\mathrm{L}}$R150 (CH1)

6. CONCLUSIONS

This paper presents the seismic response of 20-story building with viscous dampers considering the performance decrement under long-period ground motion by using 3D model. The main structure is elastic. The effect of bending deformation is not considered. The viscous dampers are evaluated for two types, medium capacity dampers and large capacity dampers. The three analysis methods, conventional method, simplified method, and detailed method, were also assessed. This paper clarified the following conclusions:

(1) The simplified method is most valuable amongst the three methods for design.

(2) The decrease rate of the large capacity damper is larger than the medium capacity damper, so the performance decrement of the large capacity damper is less than the medium capacity damper.

(3) The story drift is the larger, the decrease rate is the smaller without considering the effect of bending deformation, so the story drift angle of 1/150 is more valuable than 1/100 in the design.

Acknowledgment:

This work was supported by JST Program on Open Innovation Platform with Enterprises, Research Institute and Academia

References:

Akiyama, H., (1999). “Earthquake-Resistant Design Method for Buildings Based on Energy Balance,” gihodo shuppan Inc. [*in Japanese*]

Kasai, K., Sato, D,. Matsuda, K., and Nagayama, S., (2017) . “Variations in Synamiv Properties of Four Types of Full-scale Dampers Under Long-Duration Harmonic Loading and Their Smiplified Prediction Methods,” *AIJ Journal of Structural Engineering*, **63B**, 275-284. [*in Japanese*]

Nagayama, S., Sato, D,. Kasai, K., and Matsuda, K., (2017a). “Simplied Response Evaluation of Vibration Control Building with Viscous Dampers under Long Period Ground Motion, Part 2 : Response Evaluation Considering Change in Dynamic Properties of Viscous Damper,” *AIJ Summaries of technical papers of annual meeting*, **B-2**, 165-166. [*in Japanese*]

Nagayama, S., Sato, D,. Kasai, K., and Matsuda, K., (2017b) . “Simplied Response Evaluation of Vibration Control Building with Viscous Dampers under Long Period Ground Motion, Part 4: Time History Reponse Analysis Results,” *AIJ Summaries of technical papers of annual meeting*, **Structure-II**, 613-614. [*in Japanese*]

Sato, D,. Kasai, K., Nagayama, S., and Matsuda, K., (2018a) . “Response Evaluation Prediction of Passive Control Structure with Viscous Dampers Considering its Performance Decrement under Long-period Ground Motion,” *40th IABSE Symposium*, S4,19-26

Sato, D, and Okada, R,. (2018b) . “Response Evaluation Methods for Passive Controlled Building with Viscous Dampers Considering its Performance Decrement against Long-period Ground Motion,” *The 7th Asia Conference on Earthquake Engineering*,

Okada, R,. Sato, D,. (2018c) and Liu, X,. “Analysis on Energy of Passive Control Structure with Viscous Dmapers (Part1: Response Evaluation Method of Viscous Dampers Considering its Performance Decrement),” *AIJ Summaries of technical papers of annual meeting*, 405-408. [*in Japanese*]

Okada, R,. and Sato, D,. (2018d). “Analysis on Energy of Passive Control Structure with Viscous Dampers (Part2: Prediction Accuracy of Absorbed Energy by Viscous Damper),” *AIJ Summaries of technical papers of annual meeting*, 409-412. [*in Japanese*]

Building Research Institute (BRI), “The Main Point to Consider Long Period Ground Motion and the Concept of the Ground Motion,” 2017

Architectural Institete of Japan (AIJ) (2014). “Recommended Provision for Seismic Damping Systems applied to Steel Structures”. [*in Japanese*]

Appendix

The uniform decrease rate model is proposed. Two types of dampers, $_{M}$R100 and $_{L}$R150 are installed. The decrease rate λ is the minimum value of the decrease rate in Figure 14. λ_{min} of $_{M}$R100 is 0.63, λ_{min} of $_{L}$R150 is 0.86. According to the equation (2), the input viscous coefficient C_d of $_{M}$R100 is C_d 61.74kN·(s/mm)$^{0.38}$, and the C_d of $_{M}$R100 is168.56kN·(s/mm)$^{0.38}$.

Figure A and Figure B presents the maximum story drift angle R, and absolute acceleration Acc. of simplified method model and the uniform decrease rate model of $_{M}$R100 and $_{L}$R150. From figure A and figure B, it is shown that the response of the two model is almost the same. Therefore the uniform decrease rate model is valuable for design.

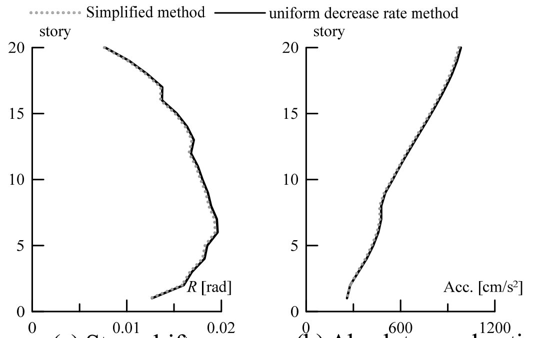

(a) Story drift (b) Absolute acceleration

Figure A Two model distributing $_{M}$R100 (λ_{min}=0.63)

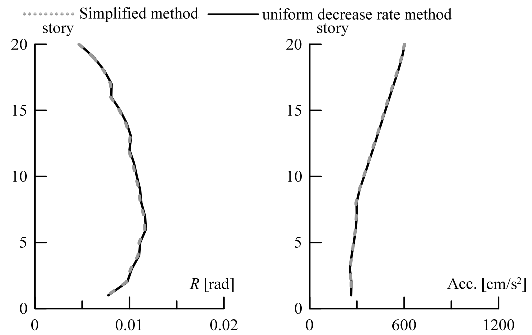

(a) Story drift (b) Absolute acceleration

Figure B Two model distributing $_{L}$R150 (λ_{min}=0.86)